JACS
JOURNAL OF THE AMERICAN CHEMICAL SOCIETY

ARTICLE

pubs.acs.org/JACS

Single-Molecule Surface-Enhanced Raman Spectroscopy of Crystal Violet Isotopologues: Theory and Experiment

Samuel L. Kleinman, Emilie Ringe, Nicholas Valley, Kristin L. Wustholz,[†] Eric Phillips,[‡] Karl A. Scheidt, George C. Schatz, and Richard P. Van Duyne*

Department of Chemistry, Northwestern University, 2145 Sheridan Road, Evanston, Illinois 60208, United States

Supporting Information

ABSTRACT: Single-molecule surface-enhanced Raman spectroscopy (SMSERS) of crystal violet (CV) has been reported since 1997, yet others have offered alternative explanations that do not necessarily imply SMSERS. Recently, the isotopologue approach, a statistically significant method to establish SMSERS, has been implemented for members of the rhodamine dye family. We provide the first demonstration of SMSERS of a triphenylmethane dye using the isotopologue approach. Two isotopologues of CV are employed to create chemically identical yet vibrationally distinct probe molecules. Experimental spectra were compared extensively with computational simulations to assign changes in mode frequencies upon deuteration. More than 90 silver nanoparticle clusters dosed with a 50:50 mixture of CV isotopologues were spectroscopically characterized, and the vibrational signature of only deuterated or undeuterated CV was observed 79 times, demonstrating that the isotopologue approach for proving SMSERS is applicable to both the CV and the rhodamine systems. The use of CV, a minimally fluorescent dye, allowed direct evaluation of enhancement factors (EF), which are reported herein. Through experiment and theory, we show that molecular electronic resonance Raman (RR) and surface-enhanced Raman effects combine synergistically in SMSERS. Excluding RR effects, the EF_{SERS} is $\sim 10^9$. Variations and relationships between substrate morphology and optical properties are further characterized by correlated SMSERS-localized surface plasmon resonance (LSPR)-high-resolution transmission electron microscopy (HRTEM) studies. We did not observe SMSERS from individual nanoparticles; further, SMSERS-supporting dimers are heterodimers of two disparately sized particles, with no subnanometer gaps. We present the largest collection to date of HRTEM images of SMSERS-supporting nanoparticle assemblies.

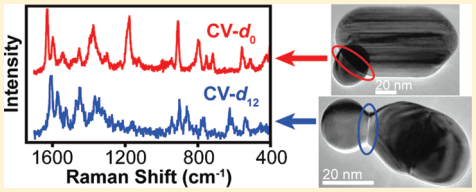

1. INTRODUCTION

Single-molecule (SM) spectroscopy is a powerful tool for monitoring both the photophysical properties of molecules as well as the effects of a local environment on molecular probes. Fluorescence spectroscopy has been used to detect single fluorophores for many years and recently has been employed in biological studies to assess cancer cell dynamics and intraprotein interactions.[1] Modulations on the frequency and intensity of molecular fluorescence can be analyzed to determine angstrom-scale distances, exemplified by the Förster resonance energy transfer technique.[2] SM studies utilizing a scanning tunneling microscope can probe electrodynamic properties of a single molecule as well as the localized area around it.[3] SMSERS, first reported in 1997,[4,5] provides rich chemical information regarding the effects of outside perturbations on the frequencies and observation of molecular vibrations. SMSERS can also support multiplexed experiments as each measurement provides a unique spectrum, which dictates molecular identity. SMSERS does not impose arbitrary restrictions on the molecular probe, such as high fluorescence quantum yield, augmenting the potential of this technique to address questions and utilize molecules, which are otherwise incompatible with more common SM methods. A greater understanding of SMSERS is still needed to facilitate the transition to the arena of applications.

The interest in SMSERS lies in its inherent analytical capabilities, the power to detect and identify an analyte down to the single molecule. For example, SMSERS has recently been used to detect a rhodamine 800 molecule with a naturally occurring ^{13}C isotope in the cyano bond. This is extraordinary because the natural distribution of carbon isotopes is nearly 99% ^{12}C and about 1.1% ^{13}C.[6] In this context, SMSERS is used to extract a vibrational signature, which is otherwise completely obscured by the ensemble. SMSERS has also been used to measure a SM Raman excitation profile for a rhodamine 6G molecule adsorbed on a silver colloidal aggregate,[7] thereby demonstrating the multiplicative nature of the surface enhancement and resonance Raman enhancement in SMSERS. Recent SMSERS reports commonly employ members of the rhodamine dye family as molecular probes, with a few notable exceptions.[8] To further illustrate the power of SMSERS, we present the results of a study on the SMSERS of CV, a nonfluorescent molecule, via an isotopically edited enhancement of the bianalyte technique, which is known as the isotopologue proof.

The bianalyte method was first introduced by Le Ru et al. in 2006 and verifies SMSERS via frequency rather than intensity correlations.[9,10] In this methodology, probe molecules with contrasting vibrational signals are deposited in low concentration on a SERS substrate. In some cases, it is possible to detect signal

Received: December 6, 2010
Published: February 24, 2011

dx.doi.org/10.1021/ja110964d | J. Am. Chem. Soc. 2011, 133, 4115–4122

distinctly from one of the two molecules even though both are present. If the SERS signal results from either molecule more frequently than both molecules at the same time, then the measurements are consistent with SMSERS. A full explanation of the statistical basis of this method is found in the literature.[8−10] This statistically significant technique has been utilized to prove the observation of SMSERS for combinations of molecules with dissimilar chemical structures (the bianalyte approach) as well as isotopically edited SERS probes (the isotopologue approach).

One assumption of the bianalyte SMSERS methodology is that a mixture will provide a SERS signal that is proportional to relative concentration in an ensemble-averaged measurement. We note that the signal would be scaled by the Raman scattering cross section of each molecule. A linear relationship between concentration and signal assumes noncompetitive and random adsorption to the SERS substrate. However, work by Deb et al. suggested that only identical pairs of isotopically modified probe molecules have SERS intensities that scale with concentration.[11] Therefore, to ensure the statistical foundation of the bianalyte model for proof of SMSERS, it is necessary to use isotopically labeled pairs of the same probe molecule, known as the isotopologue approach. Here, we use crystal violet-d_0 (CV-d_0) and crystal violet-d_{12} (CV-d_{12}) to remove uncertainty.

The CV isotopologue pair will be used to inform another ambiguity in SMSERS studies, the determination of enhancement factors (EFs). The EF is a ratio of the Raman intensity per molecule in the presence of a SERS-active substrate to normal Raman spectroscopy signal of the same molecule. CV is an ideal probe of EFs in SMSERS. It has a low fluorescence quantum yield (ϕ = 0.019)[12] and allows both normal Raman and SMSERS measurements at the same excitation wavelength (λ_{ex}), facilitating direct determination of EFs. This method is not possible in SMSERS of rhodamines due to molecular fluorescence, highlighting the need to confirm SMSERS activity for the CV system. In this work, we use both experimental and simulated Raman spectroscopy to elucidate the origins of large signal enhancements in the SMSERS of CV.

In this exploration of the SMSERS of CV, we characterize the vibrations of both CV-d_0 and CV-d_{12} using ensemble-averaged SERS coupled with time-dependent density functional theory (TDDFT) calculations. We then determine peaks that differentiate the vibrational signal of these molecules. The CV isotopologue pair is mixed with Ag colloids, and the statistics of SMSERS events are analyzed. After confirming our measurements are indeed of a single molecule, we conduct a correlated SMSERS-localized surface plasmon resonance (LSPR)-high-resolution transmission electron microscopy (HRTEM) experiment to investigate motifs in SMSERS substrate morphological and optical properties as well as their interplay with regard to plasmonic function. Fundamental studies that relate structure to function in plasmonic systems will clarify fabrication goals to create the most strongly enhancing SERS substrates.

2. EXPERIMENTAL SECTION

CV-d_{12} Synthesis. All reactions were carried out under a nitrogen atmosphere in flame-dried glassware with magnetic stirring. Reagents were purified prior to use following the guidelines of Perrin and Armarego unless otherwise stated.[13] Mass spectra data were obtained on an Agilent 6210 TOF LC/MS (ESI). The synthesis of CV-d_{12} was carried out following the reported procedure of Lohmann for CV.[14] $AlCl_3$ (20 mg, 0.15 mmol) is added to a flame-dried, one-neck, 10 mL round-bottom flask equipped with magnetic stirring bar, rubber septum, and N_2 inlet. CCl_4 (251 μL, 2.6 mmol) is added to the solid through a syringe and stirred vigorously. The reaction is heated to 70 °C. *N*,*N*-Dimethyl aniline-d_5 (970 mg, 7.7 mmol) is added to this solution through a cannula in a dropwise fashion. The reaction temperature is maintained at 70 °C for 15 min following the addition. The reaction is poured into a 50 mL Erlenmeyer flask containing 5 g of crushed ice. CV-d_{12} goes into the aqueous layer. The mixture is transferred to a separatory funnel, and the layers are separated. The organic layer is washed with three 3 mL portions of water. The aqueous layers are combined and washed with diethyl ether (5 mL) to remove unreacted starting material. The aqueous solution is transferred to an Erlenmeyer flask, and $NaHCO_3$ (100 mg) is added. The solution is filtered through a funnel with glass frit to remove $Al(OH)_3$, and then concentrated under vacuum at elevated temperature. The solid is dissolved in absolute ethanol and filtered through a funnel with glass frit. The filtrate is concentrated to afford CV-d_{12} as a blue film (109 mg, 10%).

UV−Vis Solution Absorbance Characterization. Standard solutions (10^{-6}−10^{-8} M, aq) of CV-d_0 and CV-d_{12} were created in volumetric flasks and analyzed by UV−vis absorbance spectroscopy to quantify concentration. Concentration data were also used for EF calculations. The home-built spectrophotometer consisted of a white light source (F-O Lite, World Precision Industries) fiber-coupled to a cuvette holder (CUV, Ocean Optics) with the output fiber-coupled to a visible light spectrometer (SD2000, Ocean Optics).

Ag Nanoparticle Synthesis. Synthesis followed the procedure of Lee and Meisel[15] and was carried out in glassware cleaned with aqua regia and dried in an oven. Briefly, $AgNO_3$ (90 mg) was dissolved in deionized water (500 mL, Milli-Q, 18.2 MΩ/cm) in a 1 L Erlenmeyer flask and brought to a vigorous boil with magnetic stirring. Sodium citrate (10 mL, 1%) was added, and the solution was boiled, uncovered, for 30 min. During this time, the solution changes from transparent to yellow to opaque gray-green. The solution was then allowed to cool to room temperature and diluted with water to 420 mL. The solution was transferred to a brown glass bottle where the particles remain SERS-active and stable in solution for greater than 1 month.

Ag Island Film Preparation. Ag island films (AgIFs) were prepared on piranha-cleaned and base-treated coverslips (18 mm, #1) by evaporation of Ag (6 nm, 99.99%, Kurt J. Lesker Co.) in an e-beam evaporator (AXXIS, Kurt J. Lesker Co.) at a rate of 2 Å/s. The AgIFs were incubated overnight in 1 mM ethanolic solutions of either CV-d_0 or CV-d_{12} and rinsed with ethanol prior to use.

SMSERS Sample Preparation. Samples for SMSERS were created by mixing 100 μL of equimolar amounts of aqueous CV-d_0 and CV-d_{12} (5×10^{-9} M each, total 1×10^{-8} M dye) with 1 mL of Ag nanoparticles (ca. 10^{-9} M). The dye concentration is $<1 \times 10^{-9}$ M, and on average there are 0.5 molecules of CV-d_0 and 0.5 molecules of CV-d_{12} per nanoparticle. The sample solution was diluted with 1 mL of 20 mM NaCl solution to induce aggregation and allowed to mature for 2 −7 days before spectral analysis. Approximately 10 μL of this solution was deposited on clean coverslips, dried, and immersed in a dry N_2 atmosphere in a custom flow cell for SMSERS measurements. Samples for correlated SMSERS-LSPR-HRTEM measurements were created by depositing approximately 2 μL of this solution on a TEM grid, then wicking away all solution with an absorbent wipe after ∼30 s. The TEM grid was placed on a #1 coverslip in a custom flow cell and saturated with dry N_2.

Raman Spectroscopy Instrumentation. Normal Raman spectroscopy was conducted within an hour of solution concentration quantification via UV−vis analysis. Solutions were epi-illuminated with 532 nm continuous-wave laser light (Spectra-Physics Excelsior, 100 mW) using an inverted microscope (Nikon Ti−U). A 40× objective (Nikon, Plan Fluor ELWD, DIC M, numerical aperture (NA) = 0.60) focused 1.80 mW of laser light to a probe volume of 640 fL. The

two-dimensional power density (P_{ex}) at the beam waist was determined using a scanning knife edge technique (P_{ex} = 1.01 × 10^5 W/cm^2). Scattered light was collected using the same objective, filtered for residual laser light (RazorEdge long pass 532, Semrock), and focused on the entrance slit of a 1/3 m imaging spectrograph (SP2300, Princeton Instruments). The Raman light was dispersed using a 1200 groove/mm grating and collected on a LN_2-cooled CCD (Spec10:400BR, Princeton Instruments). The same microscope and detection system was used for all spectroscopy unless otherwise noted. Experimental conditions: λ_{ex} = 532 nm, P_{ex} = 1.01 × 10^5 W/cm^2, acquisition time (t_{aq}) = 100 s.

SERS characterization of isotopologues was conducted on AgIFs incubated with CV isotopologues and mounted in a custom-built flow cell in a dry N_2 atmosphere. SERS measurements utilized an epi configuration with a 100× oil-immersion objective (Nikon, Plan Fluor, NA = 0.5−1.3) with NA set to 0.5. Experimental conditions: λ_{ex} = 532 nm, incident power (I_{ex}) = 1.65 or 1.72 mW, t_{aq} = 5 or 10 s.

SMSERS measurements were conducted by analyzing nanoparticles dosed with a mixture of CV isotopologues, which were drop-cast on clean #1 glass coverslips, allowed to dry, placed in a custom-built flow cell, and immersed in a dry N_2 atmosphere. A 100× oil-immersion objective was used with NA set to 0.5. To illuminate the entire field of view, λ_{ex} = 532 nm laser light was directed in grazing incidence geometry with a 60° angle between the surface normal and direction of light propagation. The light was focused by a 30 cm focal length lens to an elliptical spot with dimensions r_x = 198 μm and r_y = 78 μm, determined by the scanning knife edge technique. Experimental conditions: I_{ex} = 37 mW, P_{ex} = 75.9 W/cm^2, t_{aq} = 2−30 s.

LSPR Instrumentation. Broadband illumination was provided by a pillar-mounted quartz-tungsten-halogen lamp directed through a dark-field condenser (Nikon, NA = 0.8−0.95). A 100× oil-immersion objective, NA set to 0.5, collected Rayleigh scattered light from the nanoparticles, which was then sent to the spectrograph, dispersed by a 150 groove/mm grating, and collected on a CCD.

HRTEM. Support films used were Ultrathin carbon type A coated 400 mesh Cu grids obtained from Ted Pella, which have a 30−60 nm thick layer of Formvar (polyvinyl formal) on one side, and a 3−4 nm layer of amorphous carbon on the other side. The particles were applied on the Formvar side. HRTEM images were obtained within 2 days of the optical characterization on a JEOL JEM2100 FAST TEM operating at 200 kV.

EF Determination. Normal Raman spectroscopy of CV-d_0 in water and SMSERS data was processed using custom software written for MATLAB. Briefly, the data are smoothed, and a linear baseline is established for each peak. Peaks are fit to a Lorentzian line shape, and the peak area is integrated, providing a table of integrated peak areas. The following peaks were analyzed: 806, 914, 1177, 1370, 1442 rel cm^{-1}. Conversion factors related to instrument response and throughput were removed by utilizing the same laser, microscope, and detection system. A correction was applied for differences in objective NA, P_{ex}, and t_{aq}.

Computational Modeling. The electronic structure calculations presented in this work have been performed using the Amsterdam Density Functional (ADF) program package.[16] Full geometry optimization, frequency, and polarizability calculations for isolated CV-d_0 and CV-d_{12} were completed using the Becke-Perdew (BP86) exchange correlation functional and a triple-ζ polarized Slater type (TZP) basis set.

Polarizabilities were calculated using the AORESPONSE module within the adiabatic local density approximation. Polarizabilities on resonance were calculated using a global damping parameter of Γ = 0.004 au (0.1 eV), which represents a reasonable estimate of the excited state dephasing lifetime, consistent with earlier works.[17] Raman scattering cross sections were calculated by eq 1:[18]

$$\frac{d\sigma_j}{d\Omega} = \frac{\pi^2}{\varepsilon_0{}^2}(\omega - \omega_j)^4 \frac{h}{8\pi^2 c\omega_j}[45\bar{\alpha}'_j{}^2 + 7\gamma'_j{}^2]\frac{1}{45(1 - e^{(-hc\omega_j/k_B T)})} \quad (1)$$

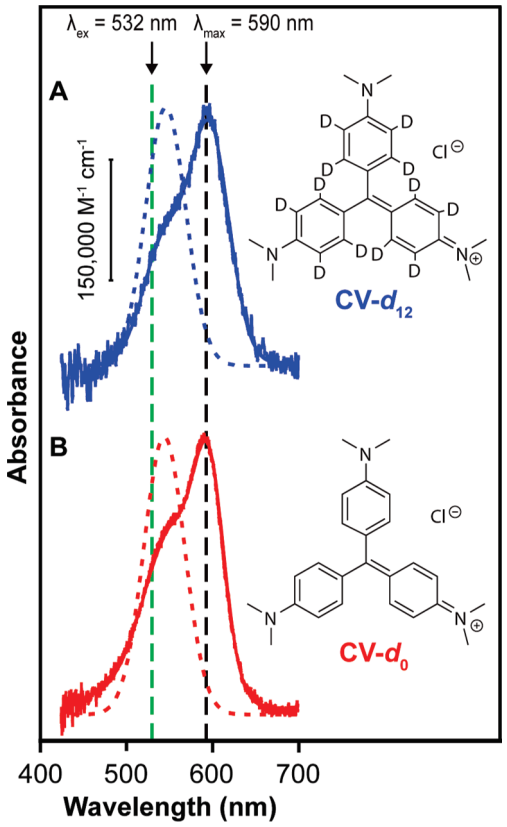

Figure 1. Structures of CV isotopologues as well as simulated (TDDFT, gas phase, dashed line) and experimental (~10^{-6} M (aq) solution, solid line) visible absorbance spectra of crystal violet isotopologues (A) CV-d_{12} and (B) CV-d_0. No major perturbation of the electronic structure upon deuteration is observed.

where ω and ω_j are the frequencies of the incident radiation and the jth vibrational mode, respectively. The scattering factor $45\bar{\alpha}'^2_j + 7\gamma'^2_j$ is composed of the isotropic ($\bar{\alpha}'_j$) and anisotropic (γ'_j) polarizability derivatives with respect to the jth vibrational mode.

Geometry optimization resulted in a D_3 symmetry propeller-shaped configuration for CV-d_0, consistent with previous experimental[19] and theoretical results.[20] As expected, CV-d_{12} has a qualitatively identical geometry. Images of CV-d_0 from our simulations are presented in Figure S1 in the Supporting Information. Transitions in simulated absorbance spectra were broadened and fit to a Gaussian distribution with a full-width-half-maximum (fwhm) of 55 nm, similar to experimentally measured linewidths. Raman intensities determined from polarizability derivatives for each vibration were broadened and fit to a Lorentzian distribution with a fwhm of 10 cm^{-1}, similar to experimentally measured linewidths. The BP86 functional routinely gives accurate frequencies for vibrational modes;[18] thus the calculated energies were not scaled.

3. RESULTS AND DISCUSSION

3.1. The Isotopologue Approach for SMSERS of Crystal Violet. The structures of the CV isotopologue pair are given in Figure 1 as well as the experimental (solid line) and simulated (dashed line) visible absorbance spectrum of each isotopologue. Both the experimental and the simulated spectra have identical line shape and absorbance maxima, indicating that the substitution has not altered the electronic structure of CV. The absorbance spectra contain a major peak centered at 590 nm and a less intense band centered ~545 nm. The simulated absorbance

dx.doi.org/10.1021/ja110964d |J. Am. Chem. Soc. 2011, 133, 4115–4122

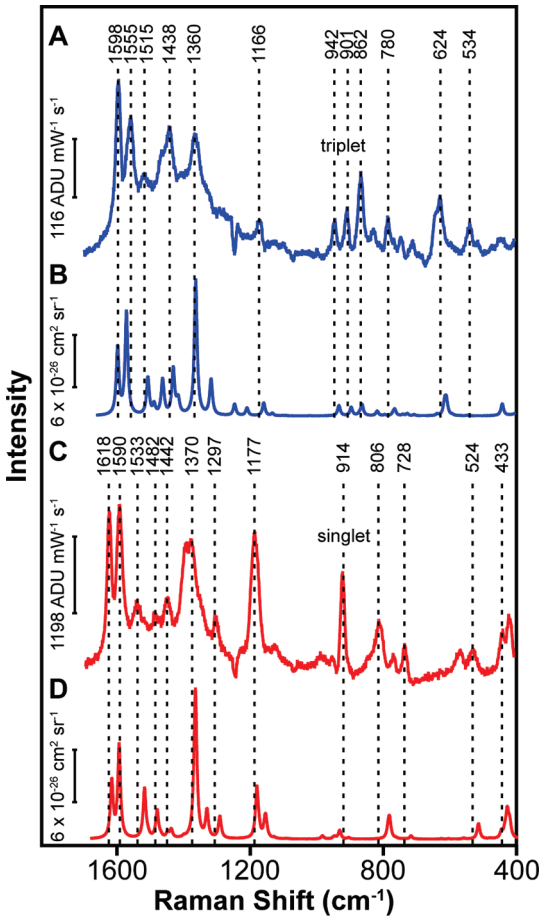

Figure 2. Simulated normal Raman and experimental SER spectra of CV-d_{12} on (A) Ag island film, (B) gas-phase TDDFT analysis; CV-d_0 on (C) Ag island film, and (D) gas-phase TDDFT analysis. SER spectra obtained using λ_{ex} = 532 nm, $t_{aq} \approx 10$ s, and $I_{ex} \approx 1.7$ mW.

spectrum of isolated CV-d_0 is composed of two nearly degenerate excitations at 545.7 and 538.6 nm with similar oscillator strengths, consistent with recent literature.[20] Raman simulations utilized λ_{ex} of 542 nm, corresponding to the peak resonance enhancement of CV in simulations, and therefore all SERS measurements and simulations are in fact resonance Raman spectroscopy; however, for agreement with previous literature, we refer to our results as SERS, not surface-enhanced resonance Raman spectroscopy. Both experimental and simulated absorbance spectra are composed of two excitations; the greater energy difference is manifested in the experimental spectrum by the presence of a shoulder at higher energy. It is important to note that the simulated spectra are gas-phase isolated CV molecules, while the experimental is in aqueous solution. For many years, the shoulder was attributed to a vibronic transition from the ground state of CV; however, recent simulated and experimental evidence has suggested that an environmental perturbation breaks the symmetry of the electronic ground state of CV, leading to two distinct excitations with disparate energies.[20] This reassignment could have significant implications in the symmetry of normal modes and their observation in SERS experiments.[21] SMSERS conducted with tunable excitation is a unique technique to explore these new assertions, although this is not the focus of this Article.

The ensemble-averaged SER spectra of CV-d_{12} and CV-d_0 on AgIFs are presented in Figure 2A and C, respectively. The

Table 1. Vibrational Frequencies of CV Isotopologue Modes

	experimental[b]			computational[b]		
assignment[a]	d_0	d_{12}	ratio	d_0	d_{12}	ratio
$\upsilon_{as,ip,C-H,\ C-\phi}$	1177	862	1.37	1181	860	1.37
$\gamma_{as,oop,\ \phi-H}$	806	624	1.29	781	605	1.29
$\upsilon_{as,\phi-C-\phi,C-N}$	1370	1360	1.01	1366	1362	1.00
ω	914	901	1.01	905	893	1.01

[a] Nomenclature for molecular vibrations is as follows: υ, stretch; as, antisymmetric; ip, in-plane; γ, bend; oop, out-of-plane; ϕ, phenyl; ω, ring breathing. [b] Frequencies in cm^{-1}.

experimental spectrum of each isotopologue show peaks in accordance with literature precedent.[22] Many subtle changes in peak frequencies and line shape occur upon deuteration; here, we focus on the most prominent features. For example, the 1625 cm^{-1} band in CV-d_0 shifts to ~1600 cm^{-1} in CV-d_{12}. However, this band is often obscured in the shoulder of another CV-d_0 peak at 1590 cm^{-1} so it is not a useful point of contrast. In the 850−950 cm^{-1} region, the CV-d_0 SER spectrum has a single intense peak centered at 914 cm^{-1}; in contrast, CV-d_{12} has three bands present in the same spectral region. The intense band at 806 cm^{-1} in CV-d_0 shifts to 624 cm^{-1} in the deuterated analogue; this band is an especially convenient point of contrast as the 600−700 cm^{-1} region is featureless in the CV-d_0 spectrum. Figure 2B,D also presents simulated resonance Raman spectra using time-dependent density functional theory (TDDFT). Scale bars for the simulated spectra relate the differential Raman cross section ($d\sigma_j/d\Omega$). We observe shifts of 5−10 cm^{-1} in vibrational frequencies between simulation and experiment. These shifts could be due to interaction with the Ag surface in the SERS experiments or because simulations are for a single isolated molecule and not an ensemble. However, the agreement between theory and experiment allows us to unequivocally relate vibrational frequencies between the isotopically edited probe molecules. The transitions around 1600, 900, and 625 cm^{-1} are used as a guide for differentiating spectra in the following SMSERS measurements.

Experimental data were compared to normal vibrational mode simulations to provide a set of peak shifts, tracking changes in vibrational energy upon deuteration. Prominent changes are highlighted in Table 1 along with ratios of peak frequencies for deuterated and nondeuterated species. Simulations demonstrated that vibrations whose energies do not change significantly upon deuteration do not invoke the motion of phenyl protons in the vibration, as expected. There are multiple peaks for which the ratios of frequencies for CV-d_0/CV-d_{12} are between 1.2 and 1.4, indicating involvement of phenyl hydrogen atoms in these vibrations, consistent with our computational results. The insight provided by ensemble averaged measurements and simulations is applied to the analysis of SMSERS events on Ag colloidal substrates.

SMSERS measurements were performed by incubating Ag colloids with equimolar concentrations of CV isotopologues, which were then diluted with NaCl solution and aged to allow moderate aggregation. Colloids were dispersed on a coverslip and illuminated with laser light using an inverted microscope. Individual diffraction-limited spots were identified by eye, and a corresponding SER spectrum was acquired. In the isotope-edited methodology, if a statistically significant number of SERS-active clusters demonstrate signal from either one or the other

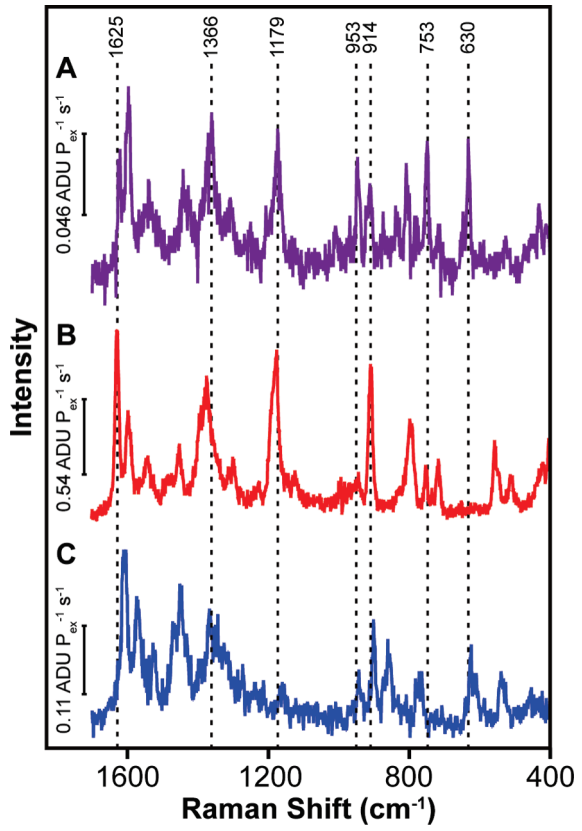

Figure 3. Representative SMSER spectra obtained using λ_{ex} = 532 nm, P_{ex} = 75.9 W/cm^2, t_{aq} = 5 s. Spectra demonstrate three distinct cases of observing (A) both isotopologues, (B) only CV-d_0, and (C) only CV-d_{12}.

isotopologue, then it can be concluded that some events originate from single molecules.[9,10] Figure 3 shows three representative SER spectra acquired from individual diffraction-limited spots. The previously highlighted peaks are used to assign spectra to one of three categories: (i) only CV-d_0, (ii) only CV-d_{12}, or (iii) both. Several aggregates produced SER spectra with spurious peaks that are attributable to citrate adducts, photodecomposition products of CV, or carbonaceous species,[23] and we removed these from the analysis. Of ~100 measurements, 53 spectra could be identified as uniquely one or the other isotopologue, or a mixture of both. A histogram of these results is presented in Figure 4. There is a minor deviation from an idealized convolution of Poisson and binomial statistics in the data. We attribute this variation to a small sample size; with more sampling, we believe the results would numerically converge to those predicted by stochastic processes. Previous literature precedent has demonstrated that the spatial mapping of SMSERS substrates coupled with automated spectral analysis can provide large data sets, which better agree with mathematical models. However, the preferential observation of either CV-d_0 or CV-d_{12} from colloids dosed with both molecules indicates we have proven the observation of SMSERS for CV-d_0 and CV-d_{12}.

3.2. The SMSERS Enhancement Factor. We assert that the augmentation of molecular polarizability via resonance Raman (RR) interactions must be considered when determining the magnitude of surface-enhancement in SMSERS, especially in studies that utilize dye molecules. Recent publications have suggested EF_{SERRS} is equal to the product of EF_{SERS} and EF_{RR}

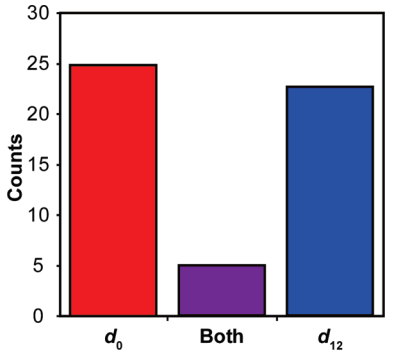

Figure 4. Histogram displaying occurrences of SER spectra from distinct isotopologues, CV-d_0 and CV-d_{12}, as well as simultaneous observation of both isotopologues. Preferential observation of just one isotopologue at a time indicates SMSERS.

($EF_{SERRS} = EF_{SERS} \times EF_{RR}$) when λ_{ex} is within the molecular electronic absorbance of a particular probe molecule.[7,24−26] The previous expression also applies to SMSERS with similarly resonant λ_{ex}. We define EF_{RR} as the ratio of the resonant and nonresonant Raman scattering cross sections, modulated by ν^4 for each excitation frequency. We now use the experimental results and TDDFT simulations to deconvolve the SERS and RR contributions to the total EF_{SERRS} in the CV system.

The EF_{RR} is nontrivial to determine experimentally. Meyer et al. have provided a thorough analysis of this problem for resonant wavelengths; however, experimentally comparing completely nonresonant λ_{ex} to fully resonant λ_{ex} has not been accomplished.[26] Therefore, we utilize simulations to assess the magnitude of EF_{RR} and experimentally investigate EF_{SERS}. Our TDDFT simulations provide a differential Raman cross section of 9.77×10^{-25} cm^2/sr for the 1620 cm^{-1} band of CV-d_0 with λ_{ex} = 542 nm. This value agrees with a previous experimental result of 2.85×10^{-25} cm^2/sr for the same band using λ_{ex} = 532 nm.[26] We also calculated differential cross sections for all modes between 200 and 2000 cm^{-1} and found the sum to be 1.15×10^{-23} cm^2/sr with λ_{ex} = 542 nm and 1.03×10^{-29} cm^2/sr with λ_{ex} = 1064 nm. We note a multiplicative factor of ~16 between these wavelengths due to the ν^4 scattering dependence. Given these considerations, simulations demonstrate that the Raman cross section of CV is augmented by an EF_{RR} of up to 10^5. The EF_{RR} is present without any surface−adsorbate interaction and is not SERS.

The EF_{SERS} values for eight SMSERS events were calculated by comparison of liquid-phase ensemble measurements of CV in solution and SMSERS on Ag colloids. This methodology, which is only possible due to the low fluorescence quantum yield of CV, accounts for and removes the EF_{RR}, allowing direct access to the EF_{SERS}. The average EF_{SERS} is 2.6×10^9 with values ranging from 2.8×10^6 to 9.3×10^{10}. The average, minimum, and maximum values were determined over all bands analyzed. These EF_{SERS} values agree with recent work on SMSERS and single nanoaggregate SERS.[27−31] The results of our experimental EF_{SERS} calculations and TDDFT simulations suggest that the SERS cross section, which enables single-molecule detection, is a synergistic result of two distinct enhancements. The EF_{RR} augments the cross section by 10^4−10^5, and the EF_{SERS} increases the observed signal by 10^6−10^{10}. It is possible that the width of the molecular excited state may be broadened upon interaction with the surface, leading to a reduction in the RR cross section.

dx.doi.org/10.1021/ja110964d |J. Am. Chem. Soc. 2011, 133, 4115–4122

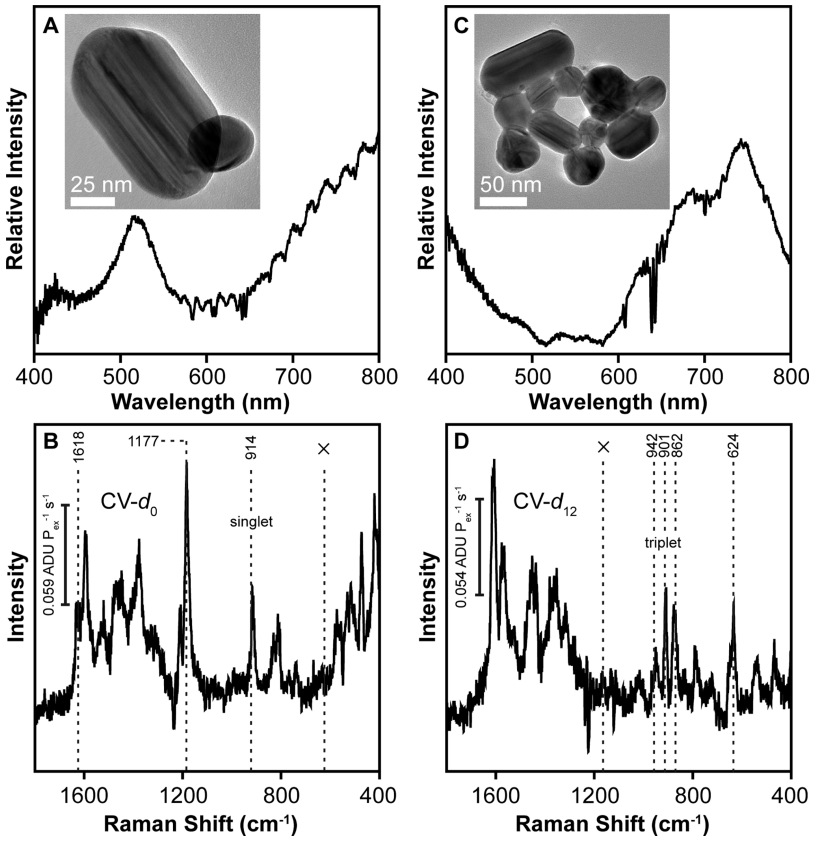

Figure 5. Correlated SMSERS-LSPR-HRTEM of isolated colloidal aggregates. (A) Dark-field scattering LSPR spectrum of Ag nanoparticle dimer with HRTEM (inset) of dimer, which supported the (B) SMSER spectrum displaying only CV-d_0. (C) Dark-field scattering LSPR spectrum of multiparticle aggregate with HRTEM (inset) of aggregate, which supported the (D) SMSER spectrum displaying only CV-d_{12}. SMSER spectra obtained using λ_{ex} = 532 nm, P_{ex} = 75.9 W/cm^2, t_{aq} = 30 s.

However, we have studied this in our past work,[24,25] and, in agreement with the present analysis, there is no indication that this is a significant factor.

3.3. Heterodimers and Higher Aggregates of Ag Nanoparticles Support SMSERS. Correlated SMSERS-LSPR-HRTEM measurements were performed by placing SMSERS-active clusters onto a TEM grid and conducting measurements as described above. Out of more than 100 spectra, 40 events demonstrated the vibrational signature of either or both CV isotopologue. Preferential observation of spectra from one or the other isotopologue confirms that the change in substrate does not affect the observation of single molecules (Supporting Information). Grid locations and relative positions of particles were used to pattern match between optical and electron microscopy images.[32] Under the experimental conditions, there should be on average one probe molecule on each nanoparticle, and yet SMSERS was observed from less than 1% of colloidal aggregates. Therefore, the aggregates that provide SMSERS signal have at least two unique attributes. First, the probe molecule is in an extremely enhancing region on the aggregate surface (i.e., "hot spot"). Second, the nanoparticle aggregate is sufficiently enhancing to support the large signal enhancements necessary to observe SMSERS. Correlated structural and spectral characterizations were performed to investigate if these morphological and plasmonic properties relate to SERS enhancing efficiency.

Figure 5 shows the correlated HRTEM image, dark-field scattering LSPR spectrum, and the resulting SMSER spectrum for two distinct nanoparticle aggregates. One aggregate is a dimer and another is composed of at least 10 nanoparticles, demonstrating the variety of nanoparticle cluster morphologies that support SMSERS. Additional HRTEM images of SMSERS-active clusters are presented in Figures S3 and S4 in the Supporting Information. The SMSERS spectra in Figure 5B,D are from different isotopologues, and no evidence for a relationship between aggregate morphology and identity of isotopologue was observed. It has been previously reported that all SMSERS-active clusters are multiparticle aggregates, necessary to create "hot spots", which are theorized to be the most highly enhancing regions of space. Consistent with previous results, SMSERS was not observed from any single particles.[33] At least four SMSERS-active clusters consisted of only two Ag nanoparticles. All SMSERS-active dimers were composed of disparately sized nanoparticles (>10% difference in radius of individual particles), and thus "heterodimer" is a more descriptive term. Additionally, it was more common to find SMSERS-active clusters of three or more Ag nanoparticles. This is expected for two reasons: one, in our sample there are a greater quantity of clusters composed of 3 or more nanoparticles than dimers, and two, there are on average more molecules per aggregate and thus a greater chance of exhibiting SMSERS. Furthermore, there was no relationship observed between SMSERS signal intensity and number of nanoparticles in an SMSERS-active cluster.

The dark-field scattering spectrum of each aggregate is also displayed in Figure 5A,C. LSPR spectra are reported for aggregates that are significantly separated from their nearest neighbors

to exclude plasmonic or diffractive coupling.[34,35] The LSPR scattering spectra demonstrate multiple peaks in locations across the visible spectrum. We have observed no correlation between the location, shape, or breadth of scattering peaks associated with SMSERS-active clusters and SMSERS signal intensity, consistent with previous work.[33] However, we present in the Supporting Information a large array of high resolution images of SMSERS-active aggregate morphologies and a sampling of LSPR scattering spectra. To our knowledge, this is the largest collection of HRTEM images of SMSERS-active clusters presented in the literature. There are many important consistencies between previous SMSERS studies on R6G and the present CV study. Fundamental studies such as these will hopefully provide insight for fabrication targets for more strongly enhancing SERS substrates.

4. CONCLUSIONS

The single-molecule surface-enhanced Raman spectroscopy of crystal violet, the second most widely investigated adsorbate after Rhodamine 6G, has been critically examined using three synergistic approaches. First, the results of a full spatially correlated isotopologue SMSERS-localized surface plasmon resonance (LSPR) spectroscopy-high resolution TEM experiments are reported. Second, unusual features in the isotopic shift pattern of the experimental SMSER spectra are understood in detail using state-of-the-art time-dependent density functional theory (TDDFT). Third, we report the value for the SERS component of the overall enhancement factor.

From this comprehensive set of experiments and the accompanying theoretical analysis, we have established several new findings relating to the isotopologue approach, the magnitude of the SERS component of the overall enhancement factor, and the structure of Ag nanoparticles that support SMSERS. The demonstrated success of the isotopologue existence proof to the crystal violet adsorbate system reinforces the generality of this approach to single-molecule surface-enhanced Raman spectroscopy. The overall enhancement factor for this surface-enhanced resonance Raman scattering (SERRS) process has been obtained using the empirically established relationship: $EF_{SERRS} = EF_{SERS} \times EF_{RR}$. The average value for EF_{SERS} was measured to be 2.6×10^9 from eight SMSERS events. EF_{RR} was estimated from TDDFT to be $\sim 10^5$ so that we can conclude that the average value of EF_{SERRS} is of order 10^{14}. The correlated SMSERS-LSPR-HRTEM experiments show that the simplest nanoparticle assembly supporting SMSERS of CV is a fused nanorod−nanosphere dimer. These results suggest that it is more likely to observe SMSERS from nanoparticle heterodimers (i.e., assemblies with differently sized and shaped particles). Furthermore, the present results add support for our hypothesis that no physical gap between two nanoparticles containing the adsorbate is required to observe SMSERS.

■ ASSOCIATED CONTENT

Supporting Information. Images of the structure of crystal violet after DFT geometry optimization, HRTEM images of SMSERS-active junctions, a histogram of SMSERS events on a TEM grid, and complete ref 15. This material is available free of charge via the Internet at http://pubs.acs.org.

■ AUTHOR INFORMATION

Corresponding Author
vanduyne@northwestern.edu

Present Addresses
[†]Department of Chemistry, College of William and Mary, Williamsburg, VA 23185.
[‡]Department of Chemistry, Yale University, New Haven, CT 06520.

■ ACKNOWLEDGMENT

This work was supported by the National Science Foundation (CHE-0802913, CHE-0911145, EEC-0647560, EEC-0634750, and DMR-0520513), AFOSR/DARPA Project BAA07-61 (FA9550-08-1-0221), and the Department of Energy Basic Energy Sciences (DE-FG02-09ER161 09).

■ REFERENCES

(1) Moerner, W. E.; Fromm, D. P. *Rev. Sci. Instrum.* **2003**, *74*, 3597–3619.
(2) Giepmans, B. N. G.; Adams, S. R.; Ellisman, M. H.; Tsien, R. Y. *Science* **2006**, *312*, 217–224.
(3) Xu, B.; Tao, N. J. *Science* **2003**, *301*, 1221–1223.
(4) Nie, S.; Emory, S. R. *Science* **1997**, *275*, 1102–1106.
(5) Kneipp, K.; Wang, Y.; Kneipp, H.; Perelman, L. T.; Itzkan, I.; Dasari, R. R.; Feld, M. S. *Phys. Rev. Lett.* **1997**, *78*, 1667–1670.
(6) Etchegoin, P. G.; Le Ru, E. C.; Meyer, M. *J. Am. Chem. Soc.* **2009**, *131*, 2713–2716.
(7) Dieringer, J. A.; Wustholz, K. L.; Masiello, D. J.; Camden, J. P.; Kleinman, S. L.; Schatz, G. C.; Van Duyne, R. P. *J. Am. Chem. Soc.* **2009**, *131*, 849–854.
(8) Blackie, E. J.; Le Ru, E. C.; Etchegoin, P. G. *J. Am. Chem. Soc.* **2009**, *131*, 14466–14472.
(9) Le Ru, E. C.; Meyer, M.; Etchegoin, P. G. *J. Phys. Chem. B* **2006**, *110*, 1944–1948.
(10) Dieringer, J. A.; Lettan, R. B.; Scheidt, K. A.; Van Duyne, R. P. *J. Am. Chem. Soc.* **2007**, *129*, 16249–16256.
(11) Deb, S. K.; Davis, B.; Ben-Amotz, D.; Davisson, V. J. *Appl. Spectrosc.* **2008**, *62*, 1001–1007.
(12) Brey, L. A.; Schuster, G. B.; Drickamer, H. G. *J. Chem. Phys.* **1977**, *67*, 2648–2650.
(13) Perrin, D. D.; Armarego, W. L. *Purification of Laboratory Chemicals*, 3rd ed.; Pergamon Press: Oxford, 1988.
(14) Lohmann, G. Y. J. . U.S. Patent 3,689,495, 1969.
(15) Park, S. K.; Lee, C. K.; Min, K. C.; Lee, N. S. *Bull. Korean Chem. Soc.* **2004**, *25*, 1817.
(16) Baerends, E. J.; et al. *ADF*, 2008.01; SCM: Amsterdam, 2009.
(17) Zhao, L.; Jensen, L.; Schatz, G. C. *J. Am. Chem. Soc.* **2006**, *128*, 2911–19.
(18) Neugebauer, J.; Hess, B. A. *J. Chem. Phys.* **2003**, *118*, 7215–7225.
(19) Dekkers, H. P. J. M.; Kielman-Van Luyt, E. C. M. *Mol. Phys.* **1976**, *31*, 1001–1019.
(20) Loison, C.; Antoine, R.; Broyer, M.; Dugourd, P.; Guthmuller, J.; Simon, D. *Chem.−Eur. J.* **2008**, *14*, 7351–7357.
(21) Canamares, M. V.; Chenal, C.; Birke, R. L.; Lombardi, J. R. *J. Phys. Chem. C* **2008**, *112*, 20295–20300.
(22) Sunder, S.; Bernstein, H. J. *Can. J. Chem.* **1981**, *53*, 964–967.
(23) Anderson, P. C.; Jacobson, M. L.; Rowlen, K. L. *J. Phys. Chem. B* **2004**, *108*, 2148–2153.
(24) Camden, J. P.; Dieringer, J. A.; Wang, Y.; Masiello, D. J.; Marks, L. D.; Schatz, G. C.; Van Duyne, R. P. *J. Am. Chem. Soc.* **2008**, *130*, 12616–12617.

(25) Zhao, J.; Dieringer, J. A.; Zhang, X. Y.; Schatz, G. C.; Van Duyne, R. P. *J. Phys. Chem. C* **2008**, *112*, 19302–19310.
(26) Meyer, S. A.; Le Ru, E. C.; Etchegoin, P. G. *J. Phys. Chem. A* **2010**, *114*, 5515–5519.
(27) Wustholz, K. L.; Henry, A. I.; McMahon, J. M.; Freeman, R. G.; Valley, N.; Piotti, M. E.; Natan, M. J.; Schatz, G. C.; Van Duyne, R. P. *J. Am. Chem. Soc.* **2010**, *132*, 10903–10910.
(28) Etchegoin, P. G.; Lacharmoise, P. D.; Le Ru, E. C. *Anal. Chem.* **2009**, *81*, 682–688.
(29) Fang, Y.; Seong, N.; Dlott, D. D. *Science* **2008**, *321*, 388–392.
(30) Franzen, S. *J. Phys. Chem. C* **2009**, *113*, 5912–5919.
(31) Le Ru, E. C.; Etchegoin, P. G.; Meyer, M. *J. Chem. Phys.* **2006**, *125*, 204701-1–204701-13.
(32) Wang, Y.; Eswaramoorthy, S. K.; Sherry, L. J.; Dieringer, J. A.; Camden, J. P.; Schatz, G. C.; Van Duyne, R. P.; Marks, L. D. *Ultramicroscopy* **2009**, *109*, 1110–1113.
(33) Michaels, A. M.; Nirmal, M.; Brus, L. E. *J. Am. Chem. Soc.* **1999**, *121*, 9932–9939.
(34) Rechberger, W.; Hohenau, A.; Leitner, A.; Krenn, J. R.; Lamprecht, B.; Aussenegg, F. R. *Opt. Commun.* **2003**, *220*, 137–141.
(35) Su, K.-H.; Wei, Q.-H.; Zhang, X.; Mock, J. J.; Smith, D. R.; Schultz, S. *Nano Lett.* **2003**, *3*, 1087–1090.